Sensors and Actuators B 212 (2015) 165–173

Contents lists available at ScienceDirect

Sensors and Actuators B: Chemical

journal homepage: www.elsevier.com/locate/snb

One-pot hydrothermal synthesis carbon nanocages-reduced graphene oxide composites for simultaneous electrochemical detection of catechol and hydroquinone

Yi Hong Huang[a], Jian Hua Chen[a,b,*], Xue Sun[a], Zhen Bo Su[a], Hai Tao Xing[a], Shi Rong Hu[a], Wen Weng[a,b], Hong Xu Guo[a], Wen Bing Wu[a], Ya San He[a]

[a] College of Chemistry and Environmental, Minnan Normal University, Zhangzhou 363000, China
[b] Fujian Province University Key Laboratory of Modern Analytical Science and Separation Technology, Minnan Normal University, Zhangzhou 363000, China

ARTICLE INFO

Article history:
Received 25 December 2014
Received in revised form 26 January 2015
Accepted 3 February 2015
Available online 12 February 2015

Keywords:
Carbon nanocages
Reduced graphene oxide
Catechol
Hydroquinone
Simultaneous determination

ABSTRACT

Facile and stable nanocomposites, carbon nanocages (CNCs)-reduced graphene oxide (RGO), were developed via one-pot in situ solvothermal reaction in this study. Transmission electron microscope, scanning electron microscope, X-ray diffraction, Raman spectroscopy, energy dispersive X-ray spectroscopy, atomic focus microscope, N_2 adsorption/desorption isotherms, thermogravimetric analysis and Fourier-transform infrared were performed to characterize the CNCs-RGO hybrid material. The electrochemical detections of catechol (CC) and hydroquinone (HQ) were investigated by means of cyclic voltammetry (CV) and differential pulse voltammetry (DPV). The excellent electrocatalytic activity and reversibility have been shown on the modified electrode toward oxidation of both CC and HQ in 0.04 M acetate buffer solution (pH = 4.0). The relationship between the oxidation peak current of CC and its concentration was linear over the range from 1 to 400 μM in the presence of 100 μM HQ, and the linear relationship between the oxidation peak current of HQ and its concentration can be obtained range from 1 to 300 μM in the presence of 100 μM CC. The detection limits (S/N = 3) for CC and HQ were 0.40 and 0.87 μM, respectively.

1. Introduction

Phenolic compounds are ubiquitous in nature since they are formed during biological degradation processes, and they are widespread used in the production of dyes, photostabilizer, developer, plasticizers, cosmetics, pesticides and some pharmaceuticals [1]. Catechol (1, 2-dihydroxybenzene, CC) and hydroquinone (1, 4-dihydroxybenzene, HQ) are two isomers of dihydroxybenzene and often coexist in environmental samples as pollutants with high toxicity and low degradation in the ecological environment [2,3]. CC and HQ are considered as environmental pollutants by the US Environmental Protection Agency (EPA) and the European Union (EU) [4]. The acceptable emission of phenolic compounds according to the national standard of China (GB 8978-1996) is 0.5 mg mL^{-1} (for dihydroxybenzene, 0.00454 M) [5]. It is difficult to separate and determine them due to the similar structures and properties of the dihydroxybenzenes [6]. Therefore, it is necessary to establish a simple, fast and reliable analytical method for sensitive and selective determination of dihydroxybenzene isomers in various matrices. A myriad of methods have been exploited to meet the rising demands for the determination of dihydroxybenzene isomers, such as liquid chromatography-ultraviolet spectrometry, [7] chemiluminescence [8], mass spectrometry [9], spectrophotometry [10], synchronous fluorescence [11] and electrochemical methods [12,13]. Among them, electrochemical methods demonstrate the merits of low cost, fast sample separation, straightforward operation and comparatively high sensitivity. However, direct determination of dihydroxybenze isomers is an obstacle for conventional electrode owing to the oxidation–reduction of the dihydroxybenzene isomers are largely overlapped in many cases [14,15]. Driven by this need, it is vital to fabricate novel electrochemical sensor for distinguish dihydroxybenzene with high sensitivity and good selectivity.

Carbon nanocages (CNCs), nanosize cage-type mesoporous carbon material with a regular framework as well as nanographene shell, have aroused considerable interest in recent years [16–18]. As a promising candidate material, CNCs are of importance in a wide range of applications including rechargeable batteries,

* Corresponding author. Tel.: +86 596 2591445; fax: +86 596 2520035.
E-mail address: jhchen73@126.com (J.H. Chen).

http://dx.doi.org/10.1016/j.snb.2015.02.013
0925-4005/

hydrogen production and storage, catalysis, sensing, and drug and gene delivery owing to their unique geometrical structure, excellent physical and electrical properties [19,20]. Up to now, the most common methods to prepare CNCs are conventional hard-templating, sacrificial templating, soft templating, and template free method [17]. Sacrificial templating method is demonstrated to introduce a porous structure into the graphitized carbon, fine polymeric or inorganic particles were served as the template for formation of carbon layers on their surfaces. From such templates with a core-shell structure, nanoporous carbons are obtained by removing the template at the core [21,22]. High-yield CNCs have been prepared by pyrolysis of ethanol and ferrous oxalate at 550 °C for 12 h in this study [23]. These CNCs with unique structural features are expected to meet the demands for electrode materials with high sensitivity, good cycling and favorable conductivity.

Since its discovery at 2004 [24], graphene, a two-dimensional (2D) one atom thick nanomaterial consisting of sp^2 hybridized carbon, has attracted considerable attention from both experimental and theoretical scientists in recent years [25]. It exhibits potential advantages of low cost, high surface area, excellent conductivity, high electrocatalytic activity, good mechanical strength, high mobility of charge carriers and extraordinary electronic transport property [26,27]. Reduced graphene oxide (RGO) is generally obtained via reduction of GO. However, RGO is hydrophobic and tends to form irreversible agglomerates due to van der Waals interactions and strong π–π stacking [28]. By incorporation of nanomaterials on the surface of RGO, the aggregation problem of RGO could be minimized or prevented [29]. Various methods have been performed to prepare RGO, and the thermal reduction of GO was proven to be an effective and reliable method to produce RGO owing to its low cost and massive scalability [30,31]. In addition, RGO supported nanocomposites have been fabricated aiming to improve electrocatalytic activities such as electron transport on modified electrode surfaces [32,33].

In this work, CNCs-RGO composites were prepared through one-pot hydrothermal method using RGO as good supports for CNCs, and their morphology and crystal structures were investigated in some details. And the CNCs-RGO composites were performed for electrochemical detection of CC and HQ.

2. Experimental

2.1. Reagents and apparatus

All reagents were attained as analytical grade and used directly without further purification. All experiments of distilled water (18.2 MΩ) was from Milli-Q plus (Millipore, USA). CC, HQ and ferrous oxalate were purchased from Aladdin (Shanghai, China). Graphite powder was obtained from Xilong Chemical Co., Ltd. (Guangdong, China). CC and HQ were respectively dissolved into distilled water to obtain 1.0 mM standard stock solution, which were further diluted by water to desired concentrations before use. Working solutions were freshly prepared by diluting the stock solution 0.2 M acetate buffer (pH = 4.5) before use and kept at 4 °C in dark.

Electrochemical experiments were carried out on a CHI 650D electrochemical workstation (Shanghai Chenhua Instruments Co., China) with a conventional three-electrode system, which contains an Ag-AgCl (saturated KCl) reference electrode, a platinum wire auxiliary electrode and a bare or modified glassy carbon electrode (GCE) as working electrode (3.0 mm diameter). All pH measurements were conducted on a Mettler Toledo FE-20 pH meter (Shanghai, China).

Transmission electron microscope (TEM) was obtained from a JEM-1230 electron microscope (FEI Tecnai G220, Ltd., USA) at 300 kV. Scanning electron microscope (SEM) was conducted on JEOL electron microscope (JEOL JSM-6010 LA, Ltd., Japan) equipped with an energy dispersive X-ray spectrometer (EDS, Japan). X-Ray diffraction (XRD) was employed to characterize GO, CNCs and CNCs-RGO nanocomposites using a Bruker D 8-Advance X-ray diractometer (Germany). The scan rate was 6° min^{-1}. Fourier-transform infrared (FTIR) spectra of GO, CNCs and CNCs-RGO nanocomposites were measured on a Nicolet 6700 FTIR instrument in the range of 800–4000 cm^{-1}. Atomic force microscope (AFM, CSPM5500, China) was allowed to observe surface morphology of GO, CNCs and CNCs-RGO. Raman spectra were obtained via Reinishaw confocal spectroscopy with 532 nm laser excitation. Thermogravimetric analysis (TGA) was carried out on TGA 209 thermal degradation analyzer (NETZSCH TG 209 F1) with a heating rate of 10 °C under N_2. N_2 adsorption/desorption isotherms were measured at 77.30 K on a Micromeritics Gemini VII 2390 volumetric adsorption system. All experiments were performed at room temperature.

2.2. Preparation of CNCs-RGO

GO was prepared according to Hummer's method [34]. The CNCs were prepared following Li's method [23]. Then, 1 mg GO was dispersed in 10 mL distilled water and ultrasonicated for 30 min to form a homogenous solution (0.1 mg mL^{-1}), followed by addition of 1.0 mg CNCs and ultrasonic agitation for 5 min. The resulting solution was put into a Teflon-lined stainless-steel autoclave of 25 mL capacity at 180 °C for 5 h, followed by natural cooling to room temperature. The precipitates were collected by centrifugation, and finally dried at 60 °C under vacuum.

2.3. Preparation of CNCs-RGO/GCE

Prior to modification, the bare GCE was polished to a mirror-like with 0.3 μm, and 0.05 μm γ-alumina slurry respectively, then washed successively with distilled water, ethanol and distilled water in an ultrasonic bath for about 3 min and dried in N_2 blowing before use. Then 5.0 μL of the CNCs-RGO (3 mg mL^{-1}) mixture solution was deposited on the fresh prepared GCE surface and allowed to dry in ambient air for 12 h to obtain CNCs-RGO modified electrode. For comparison, GO/GCE and CNCs/GCE were fabricated with the similar procedure.

3. Results and discussion

3.1. Characterization of GO, CNCs, and CNCs-RGO/GCE

The TEM image of CNCs is presented in Fig. 1a, and it shows the uniform tetragonal projected shapes and hollow structure. It indicates that the sizes of CNCs are approximately 25 nm. In addition, the lattice of CNCs is confirmed by the HRTEM image and shown in Fig. 1b. It can be observed that the lattice spacing of CNCs is 0.182 nm. The SEM image of GO and TEM image of CNCs-RGO are presented in the Fig. 1c and Fig. 1d, respectively. The typically crumpled and wrinkled structure of GO and CNCs-RGO is observed. As for Fig. 1d, it displays that CNCs is uniform distribution on RGO, indicating CNCs-RGO was successfully created by the process of hydrothermal reaction.

XRD patterns of GO, CNCs and CNCs-RGO are clearly observed in Fig. 2a. The XRD pattern of GO displays sharp diffraction peak seated at 10° corresponding to carbon (0 0 1) diffraction, which is typical in GO. It can be observed from the XRD patterns of CNCs and CNCs-RGO that two relatively low intensities of diffraction peaks located at 21° and 43° presumably assigned to (0 0 2) and (1 0 1) diffraction of hexagonal graphite (JCPDS card no. 41-1487). It indicated low crystallinity or disordered graphite of CNCs and CNCs-RGO.

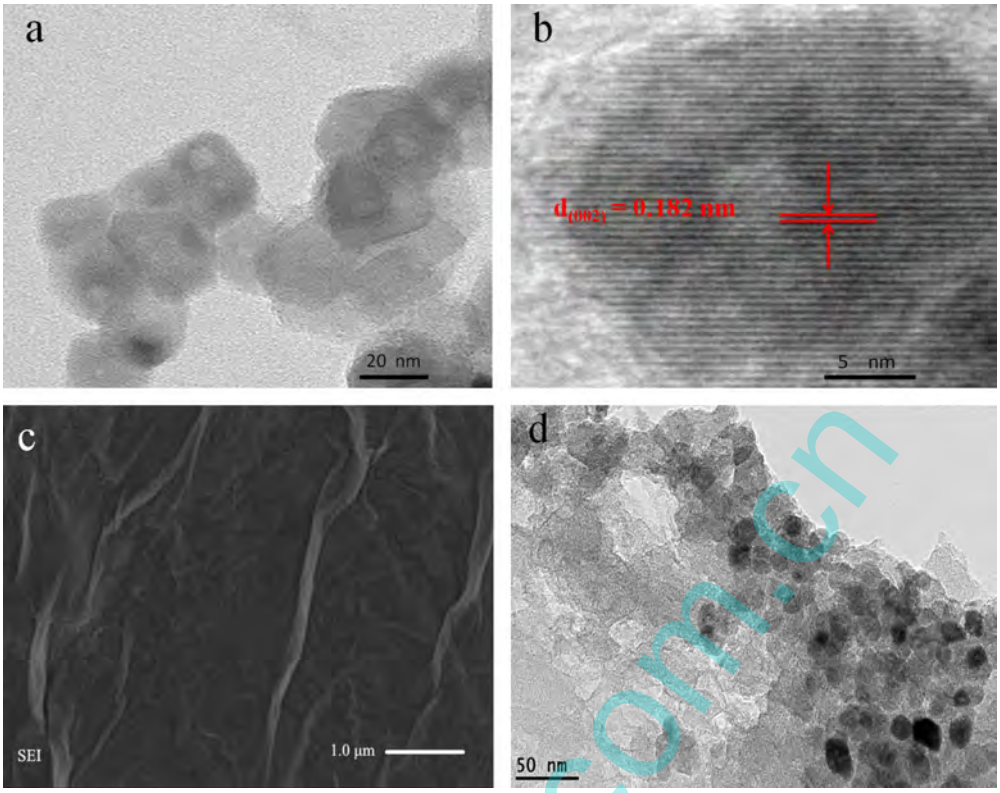

Fig. 1. TEM (a) and HRTEM (b) images of CNCs; (c) SEM image of GO; (d) TEM image of RGO-CNCs.

Raman spectroscopy was carried out to further studying graphitic structure of GO, CNCs and CNCs-RGO, and the results are present in Fig. 2b. The two strong Raman peaks situated at around 1357.67 and 1588.02 cm^{-1} are associated with the D-band (the vibration of sp^3 hybridized carbon atoms) and G-band (the vibration of sp^2 bonded carbon atoms) of GO, CNCs and CNCs-RGO. Particularly, the intensity ratio of the D-G bands implies the size of sp^2 domains and the structural disorder of GO, CNCs and CNCs-RGO

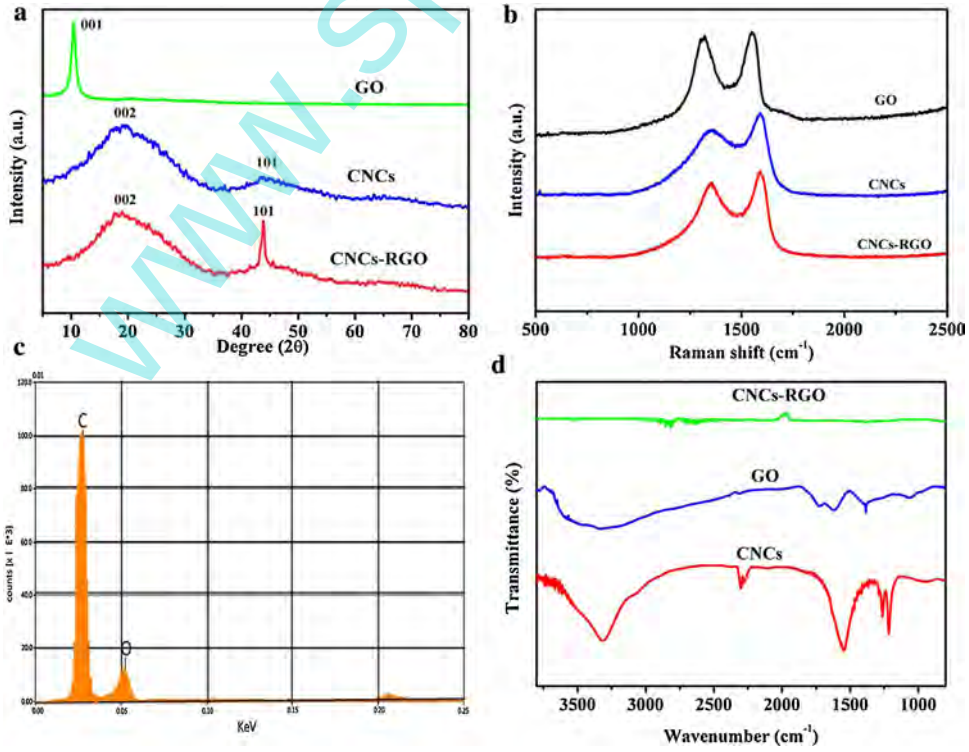

Fig. 2. XRD patterns (a), Raman spectra (b) and FTIR images (d) of GO, CNCs and CNCs-RGO; (c) EDS spectrum of CNCs-RGO sample.

[35,36]. After combining with RGO, the intensity ratio of the D-G bands for CNCs-RGO increased comparing with CNCs. This could be ascribed to the oxygen-contain groups within GO have been removed by thermal-reduction and π network has formed in the crystal structure of CNCs-RGO [37].

EDS of CNCs-RGO is confirmed and shown in Fig. 2c. It displays that major element C and O are presented in CNCs-RGO, demonstrating that GO was mostly reduced and CNCs-RGO nanocomposites were finally obtained. FTIR was also performed to characterize the major functional groups of GO, CNCs and CNCs-RGO. It can be observed in Fig. 2d that there are several characteristic peaks of various carbon-oxygen functional groups in FTIR spectrum of GO, the peaks located at ~1063 cm^{-1} and ~1232 cm^{-1} could be conform with C—O stretching vibration and C—O—C stretching vibration, and the peaks at ~1374 cm^{-1}, ~1728 cm^{-1} and ~3375 cm^{-1} should be assigned to C—OH stretching vibration, C=O in carboxylic acid and carbonyl moieties, and O—H in hydroxyl and carboxyl [34]. And the peak at ~1627 cm^{-1} could be attribute to the remaining sp^2 character. In the case of CNCs, the features in the FTIR spectrum (Fig. 2d) meet with the O—H stretching vibration at ~3432 cm^{-1}, the O—H deformation vibration at 1371 cm^{-1}, the C=C stretching vibration at 1578 cm^{-1}, and the C—C stretching vibration at 1166 cm^{-1}. After interaction with GO, it can be found that no obvious peak is observed on CNCs-RGO spectrum, indicating most reduction of GO, and CNCs have combined with GO successfully, which is consistent with the EDS result.

AFM was used to investigate surface morphology of GCE, GO/GCE, CNCs/GCE and CNCs-RGO/GCE. As displayed in Fig. S1, three dimensional of GCE, GO/GCE, CNCs/GCE and CNCs-RGO/GCE with an area of 2508 nm × 2508 nm indicated that after modification with the GO, CNCs on the GCE, the surface of the GO/GCE, CNCs/GCE became rugged comparing with the relatively flat and smooth surface of GCE. It is noted that the surface of CNCs-RGO/GCE was relatively smooth comparing with CNCs/GCE. It may be the reason that the CNCs has been combined with RGO. The dark and light areas represent the lower and higher regions on the surface. The surface roughness (Sa-Roughness average) of bare GCE, GO/GCE, CNCs/GCE and CNCs-RGO/GCE were calculated to be 0.0381, 2.242, 5.56 and 4.96 nm. These results suggest that CNCs-RGO has been decorated on the electrode interface.

TGA measurements were allowed to confirm the thermal stabilities of GO, CNCs and CNCs-RGO under a N_2 atmosphere. It can be seen from Fig. S2 that GO has the tendency to lose weight below 100 °C in virtue of the thermal decomposition of the water molecules onto the hydrophilic GO surface through physical composition. At around 200 °C, the second significant loss weight happened in this process, it may be caused by the loss of the oxygen-containing functional groups of GO [38,39]. From TGA curve of CNCs, it clarifies that the two main loss weight took place at 150 °C and 200 to 360 °C. While a sharp increase in the weight loss appeared at the temperature exceeded 360 °C, it may be the resulting of a little loss of amorphous carbon [40]. The TGA curve tend to stable when the temperature is above 410 °C, illuminating that no significant weight loss would happen in this step. The TGA curve of CNCs-RGO composite discloses the expected thermal behavior. And the phenomenon indicates that thermal stability of CNCs-RGO composite is higher than that of GO and CNCs under the temperature is below 450 °C.

Nitrogen adsorption-desorption isotherms and the corresponding pore size distribution curve of CNCs and CNCs-RGO are shown in Fig. 3. From Fig. 3a and c, one can find that the curve slowly increases at low relative pressure of 0.10–0.40, then a sharp increase occurs in the range of 0.40–0.80, which is the type-IV shape. Particularly, the existence of mesopores can be justified by the hysteresis of the desorption curve and the sharp increase of the adsorption capacity in the medium relative pressure region [41]. It can be obviously observed from Fig. 3b and d that a narrow poresize distribution was mainly concentrated on approximately 4.7 nm. It has been proven that quick molecules and ion diffusion would take place within poresize larger than 2 nm in aqueous electrolyte has been exemplified [42]. Brunauer–Emmett–Teller (BET) measurements bear out that the specific surface areas of CNCs and CNCs-RGO are 170.24 m^2/g and 388.94 m^2/g, respectively. All these results demonstrate that CNCs-RGO are prospective to have excellent electrochemical properties with increasing surface area.

3.2. Electrochemical behavior of modified electrode

The electrochemical properties of an electrode was examined at $[Fe(CN)_6]^{3-/4-}$ by cyclic voltammetry (CV). From Fig. 4a, CVs of bare GCE, GO/GCE, CNCs/GCE and CNCs-RGO/GCE in 1 mM $Fe(CN)_6^{3-/4-}$ containing 0.1 M KCl can be observed, and it is worth noting that a pair of well-defined redox peaks on CNCs-RGO/GCE with higher redox peak currents in comparison with other electrodes. As the electron transfer rate for the ferricyanide is inversely proportional to the ΔE_p [43], as a consequence of lower ΔE_p implies a higher electron transfer rate. The peak potential separation (ΔE_p) at bare GCE, GO/GCE, CNCs/GCE and CNCs-RGO/GCE are calculated to be 90, 358, 76 and 67 mV respectively. This result indicates that the k^0 value of CNCs-RGO/GCE prove to be the highest. Additionally, after the combination of CNCs and RGO, CNCs-RGO/GCE shows the highest redox peak current (I_p) among the other electrodes which may be the reason that the promotion of the electron transfer process at the modified electrode surface with improved ultrahigh surface area and good electronic conductivity [41].

Electrochemical impedance spectroscopy (EIS) was further conducted to study the interface properties of electrode surfaces. The electron transfer kinetics of $[Fe(CN)_6]^{3-/4-}$ at different electrodes are shown in Fig. 4b. In a typical Nyquist plot, EIS consists of two parts: the linear part at low frequency and semicircle part at high frequency. Linear part is diffusion controlled process, and the semicircle part is in conformity to the electron transfer resistance (Ret). It can be obtained that the Ret value for $[Fe(CN)_6]^{3-/4-}$ corresponding to the bare GCE is found to be 50 Ω. After modification with CNCs on the GO, CNCs-RGO/GCE (30 Ω) is proved to be the smallest followed by CNCs/GCE (35 Ω) and GO/GCE(4500 Ω). All these results demonstrated that CNCs-RGO film was successfully immobilized on the GCE surface, which has better electrochemical properties and promotion of electron transfer process than that of bare GCE, GO/GCE and CNCs/GCE, and these results are supported by the CV data mentioned above.

3.3. Electrocatalytic oxidation of CC and HQ

CV was used to characterize electrochemical behavior of CC and HQ at CNCs-RGO modified GCE in 0.04 M acetate buffer (pH = 4.0). The CVs of 100 μM HQ and 100 μM CC at bare GCE, CNCs/GCE, GO/GCE and CNCs-RGO/GCE are presented in Fig. 5. It can be observed that only one oxidation peaks appears at the bare GCE. It may be ascribed to the fact that the oxidation peak of CC and HQ overlap. It indicates that two phenol isomers cannot be separated by the bare GCE. In the case of GO, it cannot separate the oxidation peaks of CC and HQ either. The two distinctly well-separated oxidation peaks can be obtained from CNCs/GCE at potentials of 0.258 V and 0.371 V corresponding to the oxidation of CC and HQ, respectively. From CNCs-RGO/GCE, the two well-defined oxidation peaks are also observed. It is obvious that the oxidation and reduction peaks of CC and HQ can be separated intensively and the peak currents increased comparing with the CNCs/GCE. This can be attributed to the further promotion of the electron transfer rate of CC and HQ. It suggests that a simple and sensitive electrochemical

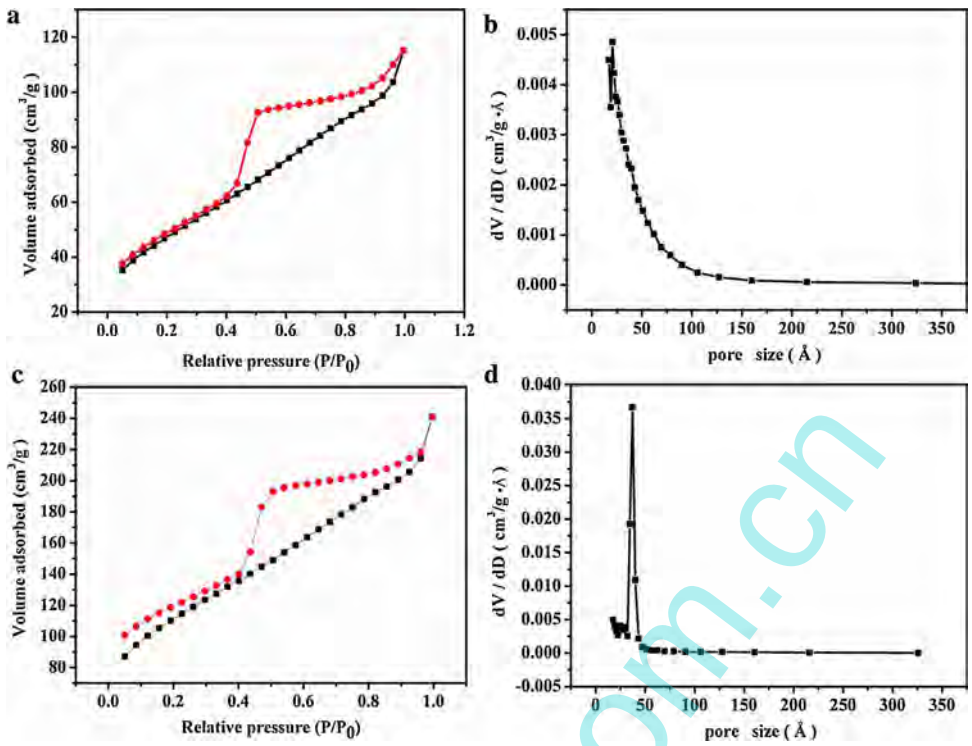

Fig. 3. Nitrogen adsorption–desorption isotherms of CNCs (a) and CNCs-RGO (c) (black and red symbols represent adsorption and desorption isotherms, respectively), and corresponding pore size distributions of the CNCs (b) and CNCs-RGO (d).

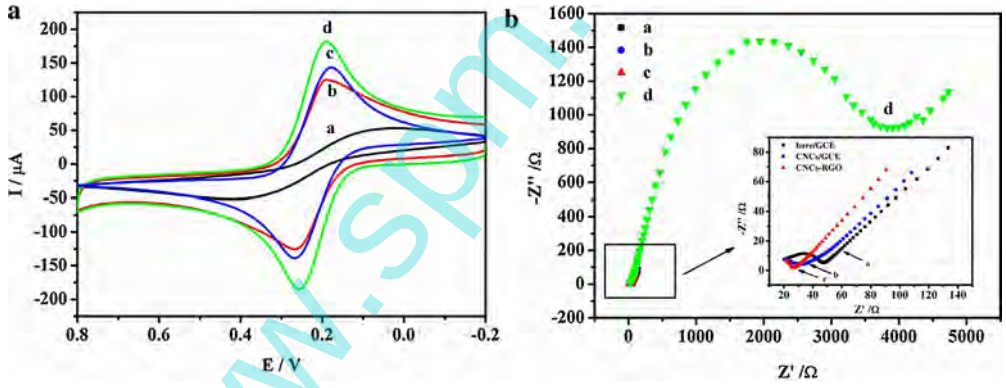

Fig. 4. a: CVs of GO/GCE (a), GCE (b), CNCs/GCE(c) and CNCs-RGO/GCE (d) in 1 mM $[Fe(CN)_6]^{3-/4-}$ (1: 1) + 0.1 M KCl at a scan rate of 100 mV s^{-1}; b: EIS of GCE (a), CNCs/GCE (b), CNCs-RGO/GCE (c) and GO/GCE(d) in 1 mM $[Fe(CN)_6]^{3-/4-}$ (1:1) + 0.1 M KCl at a scan rate of 100 mV s^{-1} and the applied ac frequency range: 0.05 Hz–100 kHz.

method exhibits promising performance for simultaneous determination of CC and HQ.

3.4. pH effect

The effect of pH value (pH 1.0–7.0) on the response of 100 μM CC and 100 μM HQ in the buffer systems at CNCs-RGO/GCE was investigated by CV and is shown in Fig. S3. The deficiency of protons would took place at higher pH value bringing about decrease the oxidation peak currents of CC and HQ with a rise in pH from 1.0 to 7.0. Additionally, the consequence of the decrease peak current values may be caused by electrostatic repulsion between the two dihydroxybenzene isomers and CNCs-RGO. The reasons should be that in the case of high pH solution, CC and HQ are apt to turn into anions, and the pKa values for CC and HQ were 9.4 and 10.3 respectively [44]. It was noted that the peak potentials of CC and HQ were verged to shift nearly to more negative values linearly with increasing of pH values, suggesting that protons participate in the electrode reaction. The linear regression equations of CC and HQ are E_{pa} (V) = 0.57974 − 0.04635 *pH* (R = 0.9929), E_{pa} (V) = 0.47636 − 0.04683 *pH* (R = 0.9935), respectively. The slopes of the two regression equations are very close to the theoretical value of 59 mV/pH for two electrons and two protons process [45,14]. It points out that electron transfer is accompanied by an equal number of protons. In addition, the pH = 4 was chosen the best optimal value, which not only drew near the pH values of the water body with strong electrochemical signals, but also with high sensitivity and good selectivity.

3.5. Effect of scan rate

The effect of scan rate on the response of 100 μM CC and 100 μM HQ in the mixed solution was also investigated by CV in the potential range from −0.2 to 0.8 V. From Fig. 6a, it can be observed that the oxidation peak potential shifts positively and the reduction peak potential shifts negatively with the increase of scan rate.

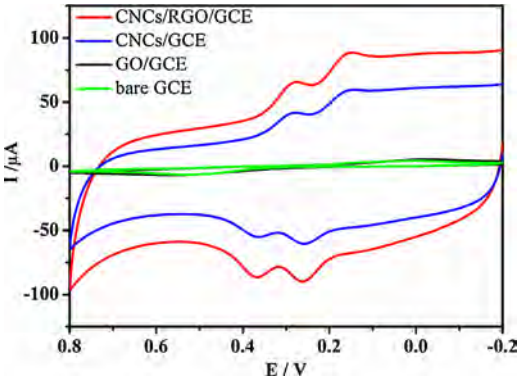

Fig. 5. CVs of 100 μM CC and HQ at bare GCE, CNCs/GCE, RGO/GCE and CNCs-RGO/GCE in 0.04 M pH 4.0 acetate buffer solution at a scan rate of 100 mV s^{-1}.

As shown in Fig. 6b and c, the redox peak currents I_{pc} and I_{pa} of CC and HQ increase linearly with square root of scan rate. The regression equations of CC (Fig. 6b) were I_{pa} (μA) = 54.342–510.614 $v^{1/2}$ ($V^{1/2}$ $s^{-1/2}$, R = 0.9911) and I_{pc} (μA) = −50.438 + 482.367 $v^{1/2}$ ($V^{1/2}$ $s^{-1/2}$, R = 0.9916). And the regression equations of HQ (Fig. 6**c**) were I_{pa} (μA) = 60.967–537.383 $v^{1/2}$ ($V^{1/2}$ $s^{-1/2}$, R = 0.9886) and I_{pc} (μA) = −41.925 +379.711 $v^{1/2}$ ($V^{1/2}$ $s^{-1/2}$, R = 0.9919). These results demonstrate that the electrochemical processes is a typical diffusion-controlled processes.

3.6. Simultaneous determination of CC and HQ

The simultaneous determination of CC and HQ at CNCs-RGO/GCE by differential pulse voltammetry (DPV) was shown in Fig. 7. Under the optimized conditions, the individual determination of CC and HQ in their mixtures was first investigated under the concentration of one species changed, whereas other specie remained constant. Fig. 7a shows different concentrations of CC in the mixtures with 100 μM HQ by DPV. A linear relationship between oxidation peak current of CC and its concentrations can be obtained. The regression equation is I_p (μA) = −0.2055 C_{CC} (μM) − 39.2129 (R = 0.9836) (inset of Fig. 7a). The detection limit for CC is estimated to be 0.40 μM (S/N = 3). In the same way, Fig. 7b displays the oxidation peak current of HQ in the presence of 100 μM CC, which is linear to its concentration with a regression equation of I_p (μA) = −0.0726 C_{HQ} (μM) − 48.7762 (R = 0.9924) (inset of Fig. 7b). The detection limit for HQ is 0.87 μM (S/N = 3). The DPV of binary mixture of CC and HQ with different concentrations was displayed in Fig. 7c. The regression equations of CC and HQ were I_p (μA) = −0.0650 C_{CC} (μM) − 47.8940 (R = 0.9951) and I_p (μA) = −0.0952 C_{HQ} (μM) − 31.7065 (R = 0.9942) respectively. Comparing with previous literatures, the modified electrode displays low detection limit and broad linear range. The results are presented in Table 1. Particularly, it is found that, although the sensing properties of detection limit and sensitivity of CNCs-RGO nanocomposites are not the best compared with some previous works, while the sensing performance of the obtained CNCs-RGO could be further improved by optimizing the synthesis conditions, such as reactant ratio, reaction temperature and reaction time, etc. [46]. Therefore, the modified electrode can behave as a promising electrode for simultaneous and sensitive determination of CC and HQ without interference with each other.

3.7. Interference effect

Some possible interferents are evaluated in the waste water. Interference effect of a myriad of species, such as 4 M of K^+, Na^+, 10 mM of Ca^{2+}, Ni^{2+}, Zn^{2+}, Fe^{2+}, Fe^{3+}, Cu^{2+}, Al^{3+}, Mg^{2+}, Cl^-, SO_4^{2-} on CC and HQ determination were performed. These results display no significant influence (signal change below 8%) on the signals of 100 μM CC and 100 μM HQ. Moreover, a certain concentrations of

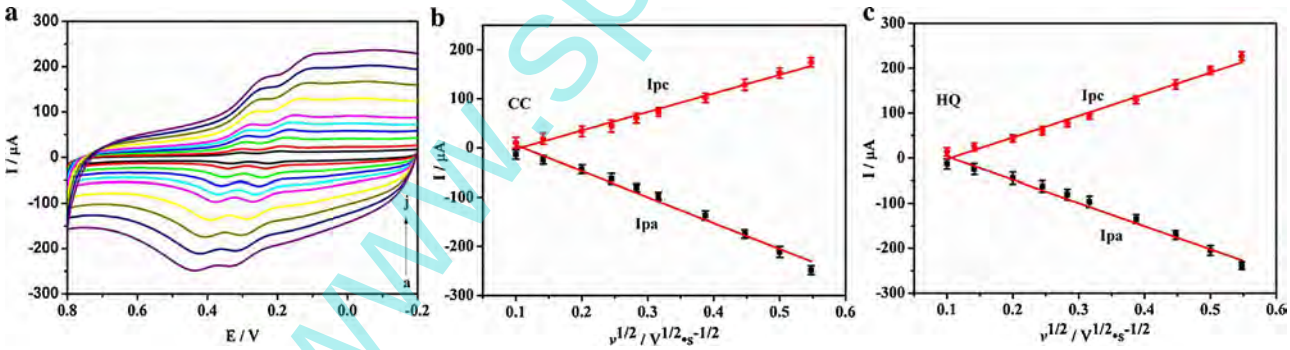

Fig. 6. (a) CV of 100 μM CC and HQ on CNCs-RGO/GCE in the pH 4.0 acetate buffer solution, redox peak current of CC (b) and HQ (c) vs. the square root of the scan rate.

Table 1
Comparison of different electrodes used in simultaneous determination of CC and HQ.

Electrode	Isomer	Detection limit (μM)	Sensitivity (μA/μM)	Linear range (μM)	Ref.
	CC HQ	0.75	0.059	1–300	[5]
		0.75	0.056	1–400	
	CC HQ	0.74	0.16	1–250	[47]
		0.62	0.19	1–230	
	CC HQ	0.20	0.417	0.5–300	[48]
		0.16	0.402	0.5–300	
	CC HQ	0.60	3.94	2–100	[49]
		0.60	3.74	2–100	
	CC HQ	1.8	0.07	5.5–540	[50]
		2.6	0.19	8–391	
	CC	0.40	0.2055	1–300	This work
	HQ	0.87	0.0726	1–400	

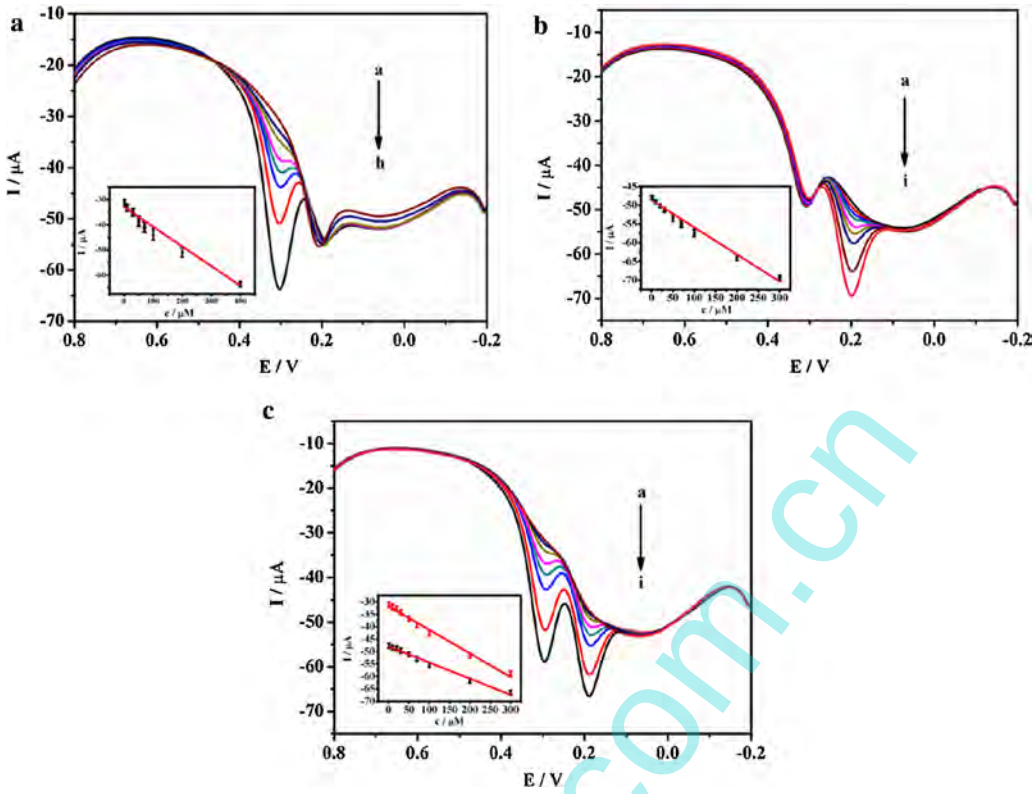

Fig. 7. (a) DPV of CNCs-RGO/GCE in the presence of 100 μM HQ with different concentrations of CC (a–h: 1, 10, 30, 50, 70, 100, 200, 400 μM) in 0.04 M pH 4.0 acetate buffer solution at a scan rate of 100 mV s^{-1}. (b) DPV of CNCs-RGO/GCE in the presence of 100 μM CC with different concentrations of HQ (a–i: 1, 10, 20, 30, 50, 70, 100, 200, 300 μM) in 0.04 M pH 4.0 acetate buffer solution at a scan rate of 100 mV s^{-1}. (c) DPV of CNCs-RGO/GCE in the presence of binary mixture of CC and HQ (a–i: 1, 10, 20, 30, 50, 70, 100, 200, 300 μM) in 0.04 M pH 4.0 acetate buffer solution at a scan rate of 100 mV s^{-1}.

Table 2
Simultaneous determination results for CC and HQ in water sample.

Samples	Tap water		Added (μM)		Found (μM)		Recovery (%)		RSD (%)	
	CC	HQ	CC	HQ	CC	HQ	CC	HQ	CC	HQ
1	0	0	5	5	5.17	4.88	103.4	97.6	0.98	1.21
2	0	0	10	10	9.75	10.34	97.5	103.4	0.56	0.33
3	0	0	15	15	15.24	14.87	101.6	99.1	0.89	1.26

phenol and resorcinol show no interference with the quantitative detection of CC and HQ.

3.8. Real sample analysis

In order to evaluate the validity of CNCs-RGO/GCE, the samples containing CC and HQ prepared from local tap water was performed. It can be seen that the prepared electrode shows selectivity and sensitivity for CC and HQ. The recoveries are in the range from 97.5% to 103.4%. The results are shown in Table 2, indicating that the proposed method could be efficiently carried out for the determination of CC and HQ.

4. Conclusions

CNCs-RGO composite film was fabricated on the bare electrode and employed for electrochemical simultaneous detection of CC and HQ. The obtained CNCs-RGO hybrid materials via synergistic effect exhibited higher film forming ability comparing with the single element, which enhanced the stability of the modified electrode. Due to the addition of CNCs to RGO, the surface of electrode becomes more porous, larger surface area and more excellent conductivity. The characterized results demonstrated that CNCs have been decorated on the RGO successfully. By taking advantage of these merits, we perform CNCs-RGO for electrochemical detection of CC and HQ. It showed excellent catalytic activity and enhanced reversibility for the electrochemical redox reaction of CC and HQ by enlarging specific surface area of CNCs-RGO and synthetic interaction between CNCs and RGO. The developed sensor elucidated encouraging selectivity and sensitivity toward CC and HQ, which has potential for further application for similar phenolic substance detection.

Acknowledgments

The authors would like to acknowledge the financial support of this work from National Natural Science Foundation of China (No. 21076174 and No. 21175115), National Natural Science Foundation of Fujian (2012J06005 and 2014J01051), and the science and technology foundation of Fujian provincial bureau quality and technical supervision (NO.FJQI2012029, NO.FJQI 2013108). The authors also thank the anonymous referees for comments on this manuscript.

Appendix A. Supplementary data

Supplementary data associated with this article can be found, in the online version, at http://dx.doi.org/10.1016/j.snb.2015.02.013.

References

[1] Y. Zhang, S. Xiao, J. Xie, Z. Yang, P. Pang, Y. Gao, Simultaneous electrochemical determination of catechol and hydroquinone based on graphene–TiO_2 nanocomposite modified glassy carbon electrode, Sensor. Actuat. B-Chem. 204 (2014) 102–108.

[2] X. Wang, M. Wu, H. Li, Q. Wang, P. He, Y. Fang, Simultaneous electrochemical determination of hydroquinone and catechol based on three-dimensional graphene/MWCNTs/$BMIMPF_6$ nanocomposite modified electrode, Sensor. Actuat. B-Chem. 192 (2014) 452–458.

[3] Y. Umasankar, A.P. Periasamy, S.M. Chen, Electrocatalysis and simultaneous determination of catechol and quinol by poly (malachite green) coated multi-walled carbon nanotube film, Anal. Biochem. 411 (2011) 71–79.

[4] X. Yang, J. Kirsch, J. Fergus, A. Simonian, Modeling analysis of electrode fouling during electrolysis of phenolic compounds, Electrochim. Acta 94 (2013) 259–268.

[5] H. Yin, Q. Zhang, Y. Zhou, Q. Ma, T. Liu, L. Zhu, S. Ai, Electrochemical behavior of catechol, resorcinol and hydroquinone at graphene-chitosan composite film modified glassy carbon electrode and their simultaneous determination in water samples, Electrochim. Acta 56 (2011) 2748–2753.

[6] M. Buleandra, A.A. Rabinca, C. Mihailciuc, A. Balan, C. Nichita, I. Stamatin, A.A. Ciucu, Screen-printed Prussian Blue modified electrode for simultaneous detection of hydroquinone and catechol, Sensor. Actuat. B-Chem. 203 (2014) 824–832.

[7] A. Asan, I. Isildak, Determination of major phenolic compounds in water by reversed phase liquid chromatography after pre-column derivatization with benzoyl chloride, J. Chromatogr. A 988 (2003) 145–149.

[8] Q. Lu, H. Hu, Y. Wu, S. Chen, D. Yuan, R. Yuan, An electrogenerated chemiluminescence sensor based on gold nanoparticles@C_{60} hybrid for the determination of phenolic compounds, Biosens. Bioelectron. 60 (2014) 325–331.

[9] Ch.I. Liao, K.L. Ku, Development of a signal-ratio-based antioxidant index for assisting the identification of polyphenolic compounds by mass spectrometry, Anal. Chem. 84 (2012) 7440–7448.

[10] P. Nagaraja, R.A. Vasantha, K.R. Sunitha, A sensitive and selective spectrophotometric estimation of catechol derivatives in pharmaceutical preparations, Talanta 55 (2001) 1039–1046.

[11] Ľ. Žiak, J. Sádecká, P. Májek, K. Hroboňová, Simultaneous determination of phenolic acids and scopoletin in brandies using synchronous fluorescence spectrometry coupled with partial least squares, Food Anal. Method. 7 (2014) 563–570.

[12] T. Gan, J. Sun, K. Huang, L. Song, Y. Li, A graphene oxide–mesoporous MnO_2 nanocomposite modified glassy carbon electrode as a novel and efficient voltammetric sensor for simultaneous determination of hydroquinone and catechol, Sensor. Actuat. B-Chem. 177 (2013) 412–418.

[13] L. Wang, Y. Meng, Q. Chen, J. Deng, Y. Zhang, H. Li, S. Yao, Simultaneous electrochemical determination of dihydroxybenzene isomers based on the hydrophilic carbon nanoparticles and ferrocene-derivative mediator dual sensitized graphene composite, Electrochim. Acta 92 (2013) 216–225.

[14] X. Feng, W. Gao, S. Zhou, H. Shi, H. Huang, W. Song, Discrimination and simultaneous determination of hydroquinone and catechol by tunable polymerization of imidazolium-based ionic liquid on multi-walled carbon nanotube surfaces, Anal. Chim. Acta 805 (2013) 36–44.

[15] Q. Guo, J. Huang, P. Chen, Y. Liu, H. Hou, T. You, Simultaneous determination of catechol and hydroquinone using electrospun carbon nanofibers modified electrode, Sensor. Actuat. B-Chem. 163 (2012) 179–185.

[16] K. Xie, X. Qin, X. Wang, Y. Wang, H. Tao, Q. Wu, L. Yang, Z. Hu, Carbon nanocages as supercapacitor electrode materials, Adv. Mater. 24 (2012) 347–352.

[17] X. Lou, L. Archer, Z. Yang, Hollow micro-nanostructures synthesis and applications, Adv. Mater. 20 (2008) 3987–4019.

[18] K. Wang, Z. Li, Y. Wang, H. Liu, J. Chen, J. Holmes, H. Zhou, Carbon nanocages with nanographene shell for high-rate lithium ion batteries, J. Mater. Chem. 20 (2010) 9748–9753.

[19] R. Zhang, M. Hummelgård, H. Olin, Carbon nanocages grown by gold templating, Carbon 48 (2010) 424–430.

[20] H. Li, Q. Yue, S. Xu, L. Wang, J. Liu, H. Li, Q. Yue, S. Xu, L. Wang, J. Liu, Fabrication of octahedral carbon nanocages via an in-situ template approach, Mater. Lett. 66 (2012) 353–356.

[21] B. Xia, J. Wang, X. Wang, J. Niu, Z. Sheng, M. Hu, Q. Yu, Synthesis and application of graphitic carbon with high surface area, Adv. Funct. Mater. 18 (2008) 1790–1798.

[22] S. Yoon, S. Lim, S. Hong, W. Qiao, D. Whitehurst, I. Mochida, B. An, K. Yokogawa, A conceptual model for the structure of catalytically grown carbon nanofibers, Carbon 43 (2005) 1828–1838.

[23] G. Li, H. Yu, L. Xu, Q. Ma, C. Chen, Q. Hao, Y. Qian, General synthesis of carbon nanocages and their adsorption of toxic compounds from cigarette smoke, Nanoscale 3 (2011) 3251–3257.

[24] K.S. Novoselov, A.K. Geim, S.V. Morozov, D. Jiang, Y. Zhang, S.V. Dubonos, I.V. Grigorieva, A.A. Firsov, Electric field effect in atomically thin carbon films, Science 306 (2004) 666–669.

[25] L.F. Dumée, C. Feng, L. He, Z. Yi, F. She, Z. Peng, W. Gao, C. Banos, J.B. Davies, C. Huynh, S. Hawkins, M.C. Duke, S. Gray, P.D. Hodgson, L. Kong, Single step preparation of meso-porous and reduced graphene oxide by gamma-ray irradiation in gaseous phase, Carbon 70 (2014) 313–318.

[26] S. Hu, Y. Wang, X. Wang, L. Xu, J. Xiang, W. Sun, Electrochemical detection of hydroquinone with a gold nanoparticle and graphene modified carbon ionic liquid electrode, Sensor. Actuat. B-Chem. 168 (2012) 27–33.

[27] H.S. Han, H.K. Lee, J.M. You, H. Jeong, S. Jeon, Electrochemical biosensor for simultaneous determination of dopamine and serotonin based on electrochemically reduced GO-porphyrin, Sensor. Actuat. B-Chem. 190 (2014) 886–895.

[28] D. Li, M.B. Muller, S. Gilje, R.B. Kaner, G.G. Wallace, Processable aqueous dispersions of graphene nanosheets, Nat. Nanotechnol. 3 (2008) 101–105.

[29] Y. Si, E.T. Samulski, Exfoliated graphene separated by platinum nanoparticles, Chem. Mater. 20 (2008) 6792–6797.

[30] Z.H. Sheng, L. Shao, J.J. Chen, W.J. Bao, F.B. Wang, X.H. Xia, Catalyst free synthesis of nitrogen-doped graphene via thermal annealing graphite oxide with melamine and its excellent electrocatalysis, ACS Nano 5 (2011) 4350–4358.

[31] S. Li, K. Qian, C. Wang, B. Hua, F. Wang, Z. Sheng, X. Xia, Application of thermally reduced graphene oxide modified electrode in simultaneous determination of dihydroxybenzene isomers, Sensor. Actuat. B-Chem. 174 (2012) 441–448.

[32] D. Chen, L.H. Tang, J.H. Li, Graphene-based materials in electrochemistry, Chem. Soc. Rev. 39 (2010) 3157–3180.

[33] T. Xu, Q. Zhang, J. Zheng, Z. Lv, J. Wei, A. Wang, J. Feng, Simultaneous determination of dopamine and uric acid in the presence of ascorbic acid using Pt nanoparticles supported on reduced graphene oxide, Electrochim. Acta 115 (2014) 109–115.

[34] C. Bao, L. Song, W. Xing, B. Yuan, C. Wilkie, J. Huang, Y. Guo, Y. Hu, Preparation of reduction graphene oxide by pressurized oxidation and multiplex reduction and its polymer nanocomposites by masterbatch-based melt blending, J. Mater. Chem. 22 (2012) 6088–6096.

[35] L.Q. Xu, Y.K. Yee, K.G. Neoh, E.T. Kang, G.D. Fu, Cyclodextrin-functionalized graphene nanosheets, and their host-guest polymer nanohybrids, Polymer 54 (2012) 2264–2271.

[36] J. Li, G. Xiao, C. Chen, R. Li, D. Yan, Superior dispersions of reduced graphene oxide synthesized by using gallic acid as a reductant and stabilizer, J. Mater. Chem. A 1 (2013) 1481–1487.

[37] Z. Wang, H. Wang, Z. Zhang, G. Liu, Electrochemical determination of lead and cadmium in rice by a disposable bismuth-electrochemically reduced graphene-ionic liquid composite modified screen-printed electrode, Sensor. Actuat. B-Chem. 199 (2014) 7–14.

[38] T.A. Pham, B.C. Choi, K.T. Lim, Y.T. Jeong, A simple approach for immobilization of gold nanoparticles on graphene oxide sheets by covalent bonding, Appl. Surf. Sci. 257 (2011) 3350–3357.

[39] X. Wang, Q. Wang, Q. Wang, F. Gao, F. Gao, Y. Yang, H. Guo, Highly dispersible and stable copper terephthalate metal-organic framework-graphene oxide nanocomposite for an electrochemical sensing application, ACS Appl. Mater. Inter. 6 (2014) 11573–11580.

[40] C.M. Chen, M. Chen, F.C. Leu, S.Y. Hsu, S.C. Wang, S.C. Shi, C.F. Chen, Purification of multi-walled carbon nanotubes by microwave digestion method, Diam. Relat. Mater. 13 (2004) 1182–1186.

[41] P. Gai, H. Zhang, Y. Zhang, W. Liu, G. Zhu, X. Zhang, J. Chen, Simultaneous electrochemical detection of ascorbic acid, dopamine and uric acid based on nitrogen doped porous carbon nanopolyhedra, J. Mater. Chem. B 1 (2013) 2742–2749.

[42] C. Liang, Z. Li, S. Dai, Mesoporous carbon materials: synthesis and modification, Angew. Chem. Int. Ed. 47 (2008) 3696–3717.

[43] R.S. Nicholson, Theory and application of cyclic voltammetry for measurement of electrode reaction kinetics, Anal. Chem. 37 (1965) 1351–1355.

[44] X. Yuan, D. Yuan, F. Zeng, W. Zou, F. Tzorbatzoglou, P. Tsiakaras, Y. Wang, Preparation of graphitic mesoporous carbon for the simultaneous detection of hydroquinone and catechol, Appl. Catal. B: Environ. 129 (2013) 367–374.

[45] H. Han, J. You, H. Seol, Electrochemical sensor for hydroquinone and catechol based on electrochemically reduced GO-terthiophene-CNT, Sensor. Actuat. B-Chem. 194 (2014) 460–469.

[46] C. Gao, X.Y. Yu, R.X. Xu, J.H. Liu, X.J. Huang, AlOOH-reduced graphene oxide nanocomposites: one-pot hydrothermal synthesis and their enhanced electrochemical activity for heavy metal ions, ACS Appl. Mater. Inter. 4 (2012) 4672–4682.

[47] L. Zheng, L. Xiong, Y. Li, J. Xu, X. Kang, Z. Zou, S. Yang, J. Xia, Facile preparation of polydopamine-reduced graphene oxide nanocomposite and its electrochemical application in simultaneous determination of hydroquinone and catechol, Sensor. Actuat. B-Chem. 177 (2013) 344–349.

[48] X. Zhou, Z. He, Q. Lian, Z. Li, H. Jiang, X. Lu, Simultaneous determination of dihydroxybenzene isomers based on graphene-reduction graphene oxide nanocomposite modified glassy carbon electrode, Sensor. Actuat. B-Chem. 193 (2014) 198–204.

[49] Y. Ding, W. Liu, Q. Wu, X. Wang, Direct simultaneous determination of dihydroxybenzene isomers at C-nanotube-modified electrodes by derivative voltammetry, J. Electroanal. Chem. 575 (2005) 275–280.

[50] F. Hu, S. Chen, C. Wang, R. Yuan, D. Yuan, C. Wang, Study on the application of reduced graphene oxide and multiwall carbon nanotubes hybrid materials for simultaneous determination of catechol, hydroquinone, p-cresol and nitrite, Anal, Chim. Acta 724 (2012) 40–46.

Biographies

Yi Hong Huang is currently a postgraduate student of Minnan Normal University, current research interest in material synthesis and analytical application.

Jian Hua Chen received his Ph.D. in Xiamen University in 2008. He is current working in College of Chemistry and Environment, Minnan Normal University as associate

professor. His research interests cover membrane material, separation, bioelectrochemistry and chemical biosensors.

Xue Sun is a postgraduate student of Minnan Normal University, majoring in Organic Chemistry.

Zhen Bo Su is a postgraduate student of Minnan Normal University, majoring in Analytical Chemistry.

Hai Tao Xing is a postgraduate student of Minnan Normal University, majoring in Analytical Chemistry.

Shi Rong Hu is a Professor of College of Chemistry and Environment, Minnan Normal University. His current research interest covers synthesis, bioelectrochemistry and chemical biosensors.

Wen Weng is a Professor of College of Chemistry and Environment, Minnan Normal University. His current research interest is organic chemistry.

Hong Xu Guo is an associate Professor of College of Chemistry and Environment, Minnan Normal University. His current research interest is inorganic chemistry.

Wen Bing Wu is a teacher of College of Chemistry and Environment, Minnan Normal University. His current research interest is inorganic chemistry and chemical engineering separation.

Ya San He is a teacher of College of Chemistry and Environment, Minnan Normal University. His current research interest is organic chemistry and membrane separation.